JCI insight

RESEARCH ARTICLE

A collagen IV–derived peptide disrupts $\alpha_5\beta_1$ integrin and potentiates Ang2/Tie2 signaling

Adam C. Mirando,[1] Jikui Shen,[2] Raquel Lima e Silva,[2] Zenny Chu,[1] Nicholas C. Sass,[1] Valeria E. Lorenc,[2] Jordan J. Green,[1,2,3] Peter A. Campochiaro,[2] Aleksander S. Popel,[1,3] and Niranjan B. Pandey[1,3]

[1]Department of Biomedical Engineering and [2]Department of Ophthalmology and The Wilmer Eye Institute, Johns Hopkins University School of Medicine, Baltimore, Maryland, USA. [3]AsclepiX Therapeutics, Inc., Baltimore, Maryland, USA.

The angiopoietin (Ang)/Tie2 signaling pathway is essential for maintaining vascular homeostasis, and its dysregulation is associated with several diseases. Interactions between Tie2 and $\alpha_5\beta_1$ integrin have emerged as part of this control; however, the mechanism is incompletely understood. AXT107, a collagen IV–derived peptide, has strong antipermeability activity and has enabled the elucidation of this previously undetermined mechanism. Previously, AXT107 was shown to inhibit VEGFR2 and other growth factor signaling via receptor tyrosine kinase association with specific integrins. AXT107 disrupts $\alpha_5\beta_1$ and stimulates the relocation of Tie2 and α_5 to cell junctions. In the presence of Ang2 and AXT107, junctional Tie2 is activated, downstream survival signals are upregulated, F-actin is rearranged to strengthen junctions, and, as a result, endothelial junctional permeability is reduced. These data suggest that $\alpha_5\beta_1$ sequesters Tie2 in nonjunctional locations in endothelial cell membranes and that AXT107-induced disruption of $\alpha_5\beta_1$ promotes clustering of Tie2 at junctions and converts Ang2 into a strong agonist, similar to responses observed when Ang1 levels greatly exceed those of Ang2. The potentiation of Tie2 activation by Ang2 even extended to mouse models in which AXT107 induced Tie2 phosphorylation in a model of hypoxia and inhibited vascular leakage in an Ang2-overexpression transgenic model and an LPS-induced inflammation model. Because Ang2 levels are very high in ischemic diseases, such as diabetic macular edema, neovascular age-related macular degeneration, uveitis, and cancer, targeting $\alpha_5\beta_1$ with AXT107 provides a potentially more effective approach to treat these diseases.

Introduction

Excessive vascular growth, instability, and leakage are critical pathophysiological events in the progression of several diseases, including neovascular age-related macular degeneration (NVAMD), diabetic macular edema, cancer growth and metastasis, and uveitis and other inflammatory diseases (1–4). The angiopoietin (Ang)/Tie system (reviewed in refs. 5, 6) has emerged as a major regulator of vascular homeostasis and a promising therapeutic target. In quiescent vessels, paracrine release of angiopoietin 1 (Ang1) from perivascular cells stimulates Tie2 clusters across endothelial cell (EC) junctions, leading to the activation of the antiapoptotic Akt and reduced permeability through actin rearrangement and dephosphorylation of MLC2 by the Rap1 pathway (7–9). Alternatively, stimulation of Tie2 at the EC–extracellular matrix (EC-ECM) interface induces proliferation by ERK1/2 and migratory responses via Dok2 activities (8, 10). In contrast, angiopoietin 2 (Ang2) is essential for angiogenesis where it is rapidly released from Weibel-Palade bodies stored within ECs and destabilizes the vasculature by antagonizing the activities of Ang1. Ang1 inhibition leads to reduced perivascular coverage and either vessel regression or angiogenesis in the absence or presence of other growth factors, respectively (11, 12). In many disease states, the concentrations of the 2 angiopoietins are heavily skewed in favor of Ang2, which contributes to the progression of several vascular diseases through pathological increases in vessel permeability and instability (13–15). In some conditions, Ang2 may also function as a weak agonist of Tie2. Specifically, the activation of junctional Tie2 by both Ang1 and Ang2 is enhanced when the receptor is associated with the Tie1 coreceptor and cleavage of Tie1 during inflammation is suspected to regulate the agonistic and

Conflict of interest: NBP is the Head of R&D, JJG is the CTO, ASP is the CSO, and PAC is a consultant of AsclepiX Therapeutics, Inc. The terms of these arrangements are being managed by the Johns Hopkins University in accordance with its conflict-of-interest policies.

Submitted: May 7, 2018
Accepted: January 11, 2019
Published: February 21, 2019

Reference information:
JCI Insight. 2019;4(4):e122043.
https://doi.org/10.1172/jci.insight.122043.

antagonistic activities of Ang2 (16). However, understanding of the mechanism by which Ang2 switches between agonistic and antagonistic activities remains incomplete.

Both Tie receptors form complexes with the endothelial integrins $\alpha_5\beta_1$ and $\alpha_v\beta_3$ on the surface of cells. Interactions between $\alpha_5\beta_1$ integrin and Tie2 ectodomains sensitize the receptor to activation by Ang1 and are enhanced in the presence of fibronectin (FN1) (10, 16, 17). Activated Tie2 in these complexes stimulates promigratory and proliferative downstream pathways associated with FAK, Rac1, and ERK1/2 (MAPK) (10, 17). However, Ang1-mediated phosphorylation of the survival signaling factor Akt demonstrates context-specific activation by integrins. Downregulation of β_1 integrin with siRNA reduced the phosphorylation of S473 on Akt in ECs treated with COMP-Ang1, while another study showed no changes in the phosphorylation of Akt T308 following the reduction of α_5 integrin (10, 16). Whether these differences are related to the specific phosphorylation sites, the integrins targeted, cell culture methods, or underlie a more complicated relationship between integrins and Tie signaling remains to be determined and emphasizes the need for further investigation into the relationship between integrins and Ang/Tie signaling.

Here, we examine the regulatory function of integrins in Ang/Tie signaling using an integrin-binding, disruptive peptide, AXT107. AXT107 is a 20-mer natural amino acid peptide originally derived from a sequence in type IV collagen that was found in our previous work to bind tightly to integrins $\alpha_5\beta_1$ and $\alpha_v\beta_3$ and disrupt the activities of their associated growth factor receptors VEGFR2, cMet, PDGFRβ, and IGF1R (18, 19). This peptide disrupts interactions between IGF1R and β1 integrin, enhances VEGFR2 degradation in vitro, and inhibits the growth and permeability of neovascularization in vivo. In the present work, we demonstrate that AXT107 potentiates the normally weak agonistic activity of Ang2 towards Tie2 both in vitro and in vivo and specifically activates downstream targets associated with EC survival and barrier function. Mechanistically, AXT107 treatment dissociates α_5 and β_1 integrins, resulting in the translocation and activation of Tie2 at EC-EC junctions and decreased monolayer permeability and leakage through the reorganization of F-actin and VE-cadherin. These data emphasize a clear regulatory role for integrins in Tie2 signaling. AXT107 may represent a novel therapy that, rather than directly inhibiting detrimental Ang2 signaling like other agents in development that target the Ang2 signaling pathway, instead takes advantage of the high concentration of Ang2 in disease to potentiate its beneficial effects, in association with endogenous Ang1.

Results

AXT107 potentiates the activation of Tie2 by Ang2. To investigate the effects of the integrin inhibitor AXT107 on Tie2 signaling, we treated confluent monolayers of microvascular ECs (MECs) with various concentrations of AXT107 followed by exposure to the Tie2 ligands Ang1 and Ang2. Consistent with previous reports, 200 ng/ml Ang1 induced phosphorylation of Tie2 (Figure 1, A and C), while 200 ng/ml Ang2 had no effect (Figure 1, B and D). Treatment with AXT107 showed a minor, but significant decrease in Tie2 phosphorylation in Ang1-stimulated cells at the highest dose tested but did not influence the phosphorylation of the downstream, prosurvival effector Akt. Conversely, strong and significant dose-dependent increases in Tie2 and Akt phosphorylation were observed in cells treated with a combination of AXT107 and Ang2. However, the phosphorylation of the proliferation-associated factor ERK1/2 remained constant in all tested conditions. The total protein levels of Tie2 and its downstream targets remained unchanged for both Ang1 and Ang2 at all concentrations of AXT107 (Supplemental Figure 1, A and B; supplemental material available online with this article; https://doi.org/10.1172/jci.insight.122043DS1) and phosphorylation was not induced by AXT107 alone (Supplemental Figure 1C). Since AXT107 altered the effects of Ang2 more dramatically than Ang1, and the Ang1-to-Ang2 ratio is skewed towards Ang2 in diabetic macular edema, NVAMD, uveitis, cancer, and other ischemic diseases, subsequent experiments focused on Ang2.

AXT107-mediated changes in Tie2 cellular distribution influence receptor activation. Our observations that AXT107 stimulates the Ang2-mediated phosphorylation of Akt but not ERK 1/2 suggests that AXT107 may activate junctional Tie2 instead of receptors at the cell-ECM interface (20). Previously, it was reported that Tie2 at the junctions formed actin-rich complexes that were insoluble in Triton X-100–based lysis buffers but were soluble when distributed over the surface of the cell (8). Therefore, we treated MEC monolayers with various combinations of AXT107, Ang1, and Ang2 (Figure 2A) and fractionated the cell lysates by their solubility in Triton X-100–containing buffers. We also included $VEGF_{165}$ in these assays since VEGFR2 signaling often opposes the activities of Tie2. In all cases, 100 μM AXT107 was used for the clearest results. We found that increased amounts of Tie2 were in the

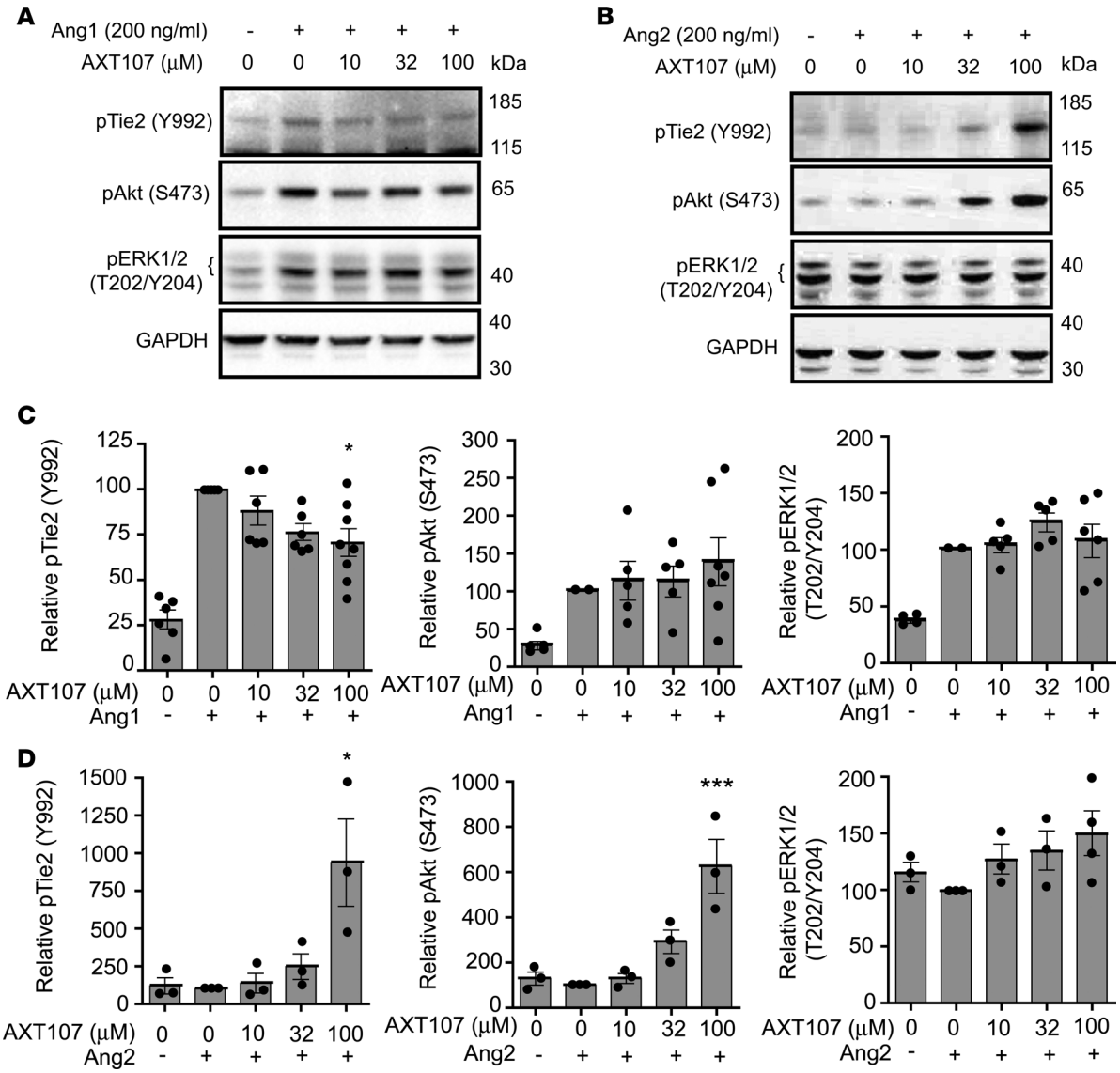

Figure 1. AXT107 potentiates the activation of Tie2 by Ang2. (**A** and **B**) Representative Western blots of MEC lysates treated with 200 ng/ml Ang1 (n = 6–8) (**A**) or 200 ng/ml Ang2 (n = 3) (**B**) and 0–100 μM AXT107 showing phosphorylation of Tie2 (Y992) and downstream effectors Akt (S473) and ERK1/2 (T202/Y204), with GAPDH as a loading control. (**C** and **D**) Densitometric analysis of Western blots described in **A** (**C**) and **B** (**D**) adjusted for loading control and presented relative to Ang1- or Ang2-alone control. *P < 0.05, ***P < 0.001 by 1-way ANOVA relative to Ang1- or Ang2-alone control.

insoluble fraction of lysates treated with AXT107, independent of growth factor treatment. Next, we wanted to determine if this relocation of Tie2 to the insoluble fraction was important for its activation by Ang2. Tie2 was immunoprecipitated from fractionated MEC lysates exposed to Ang2 with or without AXT107 and then immunoblotted for phospho-Tie2. Phosphorylation was observed only in the insoluble fractions of AXT107-treated samples (Figure 2B). Surprisingly, the total Tie2 was also consistently lower in the soluble fraction. While care was taken to keep the volumes of the soluble and insoluble fractions as identical as possible, the relative protein content could not be estimated prior to gel loading, as AXT107 contributes to the overall protein concentration. To independently confirm that phospho-Tie2 was indeed higher at the junctions after treatment with AXT107, we investigated the effects of AXT107 on the location of phospho-Tie2 in MEC monolayers by immunofluorescence microscopy using the tight junction–associated protein ZO-1 as a junctional marker (Figure 2C). In samples treated with Ang2 alone, phospho-Tie2 was predominantly found in weak, punctate distributions across the cell surface. Treatment with AXT107 increased the overall fluorescence intensity and redistributed phospho-Tie2 along cell-cell junctions. A similar redistribution could also be observed for

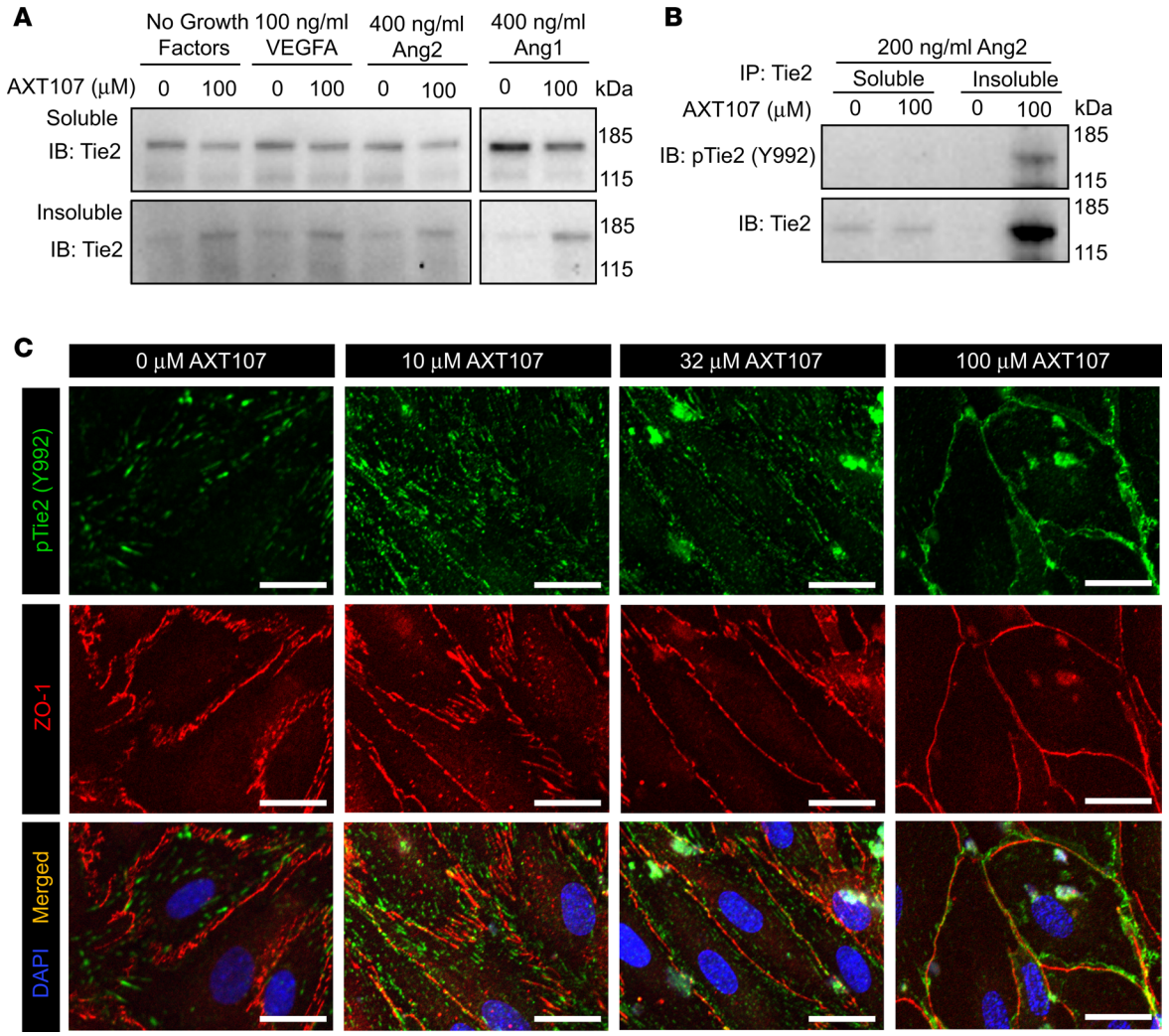

Figure 2. AXT107 alters Tie2 intracellular distribution. (**A**) MEC lysates were treated with various growth factors and 100 μM AXT107 or DMSO vehicle and fractioned into Triton X-100–soluble and –insoluble pools. Blots were stained for total Tie2 (n = 3). (**B**) Representative images of Triton X-100–fractionated lysates immunoprecipitated for Tie2 and blotted for phospho-Tie2 (top) and total Tie2 (bottom); n = 3. (**C**) Immunofluorescence images of MEC monolayers treated with 200 ng/ml Ang2 for 15 minutes at varying concentrations of AXT107 and stained with DAPI (blue) and for phospho-Tie2 (Y992) (green) and ZO-1 (red) (n = 3). Scale bars: 25 μm.

total Tie2 (Supplemental Figure 2). Interestingly, the arrangement of ZO-1 also changed in appearance from jagged and discontinuous to smooth and continuous with increasing concentrations of AXT107. Such changes are associated with tighter intercellular junctions, an effect that was further investigated and described in greater detail below.

We also investigated the effects of AXT107 on Tie1, a Tie2 coreceptor shown to be essential for the activation of junctional Tie2 (16, 21), and VE-PTP, a junctional tyrosine phosphatase that dephosphorylates Tie2. In previous reports, inhibition of VE-PTP was found to increase the activation of Tie2 by Ang2 (22). However, AXT107 treatment did not appear to alter the interactions of Tie2 with either coreceptor. Populations of Tie1 were found to relocate to the insoluble fraction after peptide exposure (Supplemental Figure 3A) and remained associated with Tie2 (Supplemental Figure 3B). VE-PTP was always found in the insoluble fraction regardless of treatment (Supplemental Figure 3C) and associated with Tie2 at the junctions (Supplemental Figure 3B). We next focused our attention on the mechanisms by which AXT107 affects integrins to elicit its effects on Ang2, Tie2, and EC-EC junctions.

AXT107 disrupts interactions between α_5 and β_1 integrin subunits. We previously identified integrins $\alpha_5\beta_1$ and $\alpha_v\beta_3$ as the primary targets of AXT107 (19). To investigate the possibility of an integrin-mediated mechanism for regulating Tie2, immunoblots of fractionated MEC lysates for the α_5 integrin subunits were used.

While the majority of the α_5 integrin subunit population remained in the soluble fraction, a portion relocated to the insoluble fraction in samples treated with AXT107, similar to what was observed for both Tie1 and Tie2 (Figure 3A). Surprisingly, the β_1 integrin subunit was never observed in the insoluble fraction (Figure 3B) despite the use of long exposure times, high antibody concentrations, and a second antibody targeting a separate epitope of β_1 integrin (Supplemental Figure 4), indicating that treatment with AXT107 disrupts interactions between the α_5 and β_1 integrin subunits. Furthermore, since β_1 is the only known β subunit to interact with α_5 integrin, it is unlikely that the α_5 subunit observed in the insoluble fractions of this assay originated from a different heterodimeric integrin pair.

Given our unprecedented observation that AXT107 dissociates the $\alpha_5\beta_1$ integrin heterodimer, we wanted to confirm this result in several independent assays. We used the Duolink proximity ligation assay to visualize individual interactions between α_5 and β_1 integrin subunits as distinct spots by fluorescence microscopy. These studies revealed that the interactions between α_5 and β_1 integrin subunits were significantly reduced in monolayers treated with AXT107 compared with vehicle alone (Figure 3, C and D). We further investigated the interactions between α_5 and β_1 integrins by coimmunoprecipitation. Pull-down of α_5 integrin in Triton X-100–fractionated lysates revealed that while α_5 integrin could be observed in the insoluble fraction after AXT107 treatment, interactions with β_1 were only found in the soluble fractions (Figure 3E). The α_5 integrin subunits that remained in the soluble fractions after AXT107 treatment, however, were still in complexes with β1 integrin, suggesting that only a specific population of $\alpha_5\beta_1$ integrins were disrupted by the peptide. We next wanted to determine if the α_5 integrin subunits in the insoluble fraction were associated with Tie2 following their separation from β_1 integrins. As shown in Figure 3F, α_5 integrin was observed in the peptide-treated, insoluble fraction following immunoprecipitation of Tie2.

AXT107 strengthens EC-EC contacts and reduces monolayer permeability. Tie2 signaling is a major regulator of vascular permeability and dysfunction in this pathway is known to contribute to increased macular edema and disease progression. Specifically, Tie2 strengthens cell-cell junctions through the formation of trans-associations between Tie2 receptors on adjacent cells and the reorganization of VE-cadherin complexes continuously along cell-cell junctions (20). Immunofluorescence imaging revealed clear changes in the structure of VE-cadherin junctions between ECs (Figure 4A). At lower concentrations the distribution of VE-cadherin was discontinuous and jagged in appearance but became progressively smoother with increasing concentrations of AXT107. The jaggedness of these junctions is related to the structural arrangement of actin fibers within the cell (Figure 4A, center row). In the absence of AXT107 treatment, actin was arranged as radial fibers that crossed much of the inside of the cells. This arrangement creates tension that pulls against the cell-cell junctions and makes the VE-cadherin distribution appear jagged. In contrast, increasing concentrations of AXT107 rearranged actin to the periphery of the cell, which applies tension along the junction, creating the consistent and smooth appearance. As a simple metric for this change in actin distribution, we calculated the average area of actin fluorescence signal per cell (Figure 4B). The total level of VE-cadherin, however, remained unchanged after 3 hours of AXT107 and Ang2 treatment (Figure 4C). As noted above, the tight junction–associated protein ZO-1 showed responses to AXT107 treatment similar to those of VE-cadherin (Figure 4D). The reorganization of VE-cadherin, ZO-1, actin, and Tie2 at EC junctions by AXT107 suggests that it stabilizes and tightens cell-cell interactions and, consequently, should reduce the permeability of molecules across the monolayer.

The effect of the peptide on EC permeability was investigated by the transendothelial diffusion of FITC-labeled dextran across MEC monolayers seeded onto permeable Transwell supports (Figure 4, E and F). Treatment with Ang2 or AXT107 alone did not influence FITC-dextran diffusion across the monolayer, whereas VEGF treatment appeared to increase permeability (although nonsignificantly) alone or in combination with Ang2. Interestingly, the addition of Ang2 alone or in combination with VEGF to monolayers preincubated with 100 μM AXT107 caused a significant decrease in FITC-dextran diffusion into the top chamber when compared with cells treated with the growth factors alone. A similar trend was also observed between monolayers treated with VEGF in the presence and absence of peptide; however, the high variability in monolayer permeability in vitro prevented significant differences.

As a potential mechanism for this actin rearrangement, phosphorylation of Tie2 is known to stimulate the Rap1 GTPase pathway, leading to a reduction in the phosphorylation of the downstream motor protein myosin light chain 2 (MLC2) that is associated with actin rearrangement (9). In support of this hypothesis, the phosphorylation of MLC2 was reduced in a dose-dependent manner following treatment with AXT107 and Ang2 (Figure 5, A and B) but not in the presence of AXT107 alone (Supplemental Figure 5A).

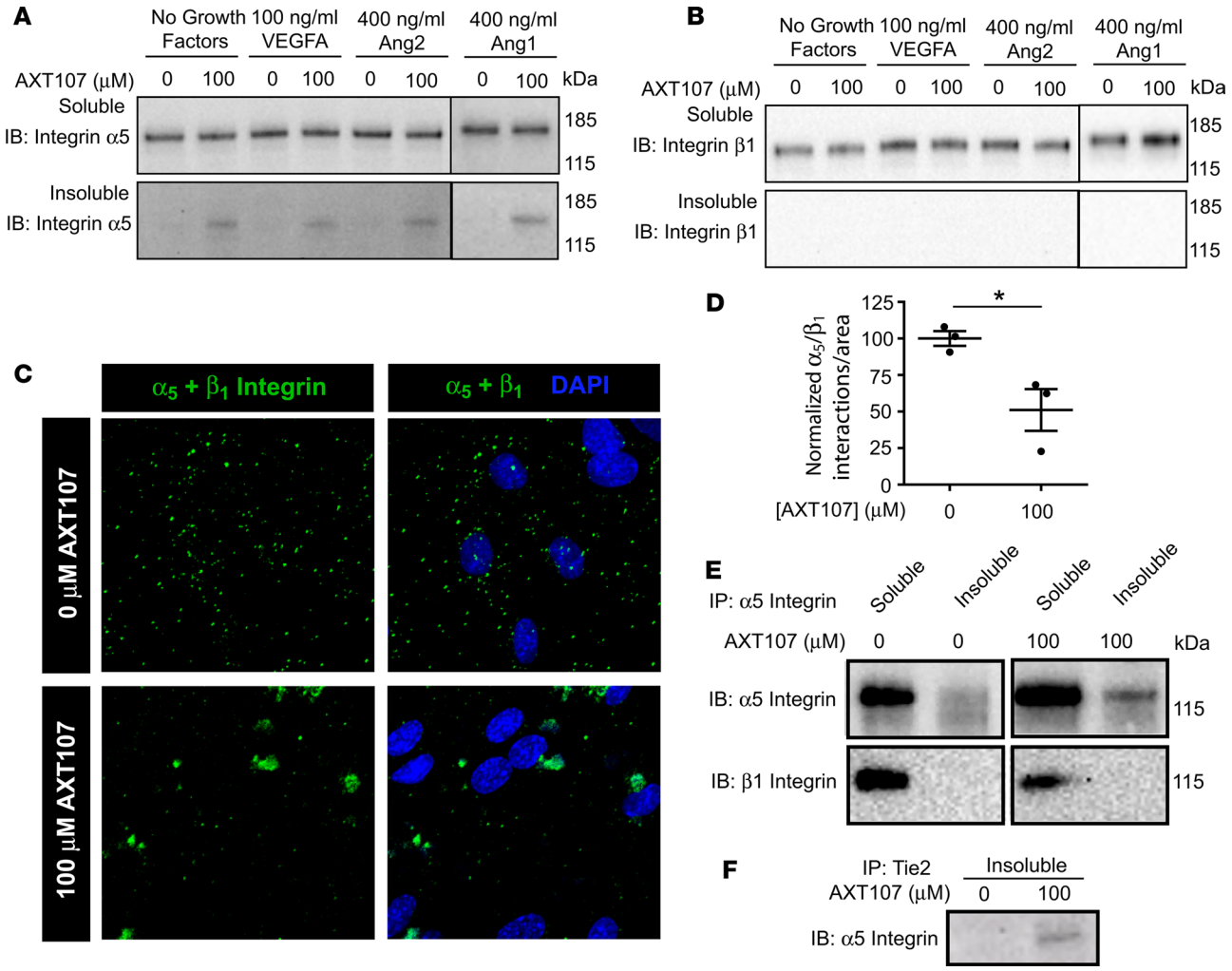

Figure 3. AXT107 disrupts interactions between α_5 and β_1 integrin. (**A** and **B**) MEC lysates were treated with various growth factors and 100 μM AXT107 or DMSO vehicle and fractioned into Triton X-100–soluble and –insoluble pools and blotted for α_5 (n = 3) (**A**) or β_1 (epitope corresponding to a site within aa 76–256) (n = 3) (**B**) integrins. (**C**). Representative images of a Duolink assay showing interactions between α_5 and β_1 integrins in MEC monolayers treated with 100 μM AXT107 or vehicle (n = 3). Scale bars: 25 μm. (**D**) Quantification of interactions per arbitrary area. (**E**) Representative blots of Triton X-100–fractionated lysates immunoprecipitated for α_5 integrin and blotted for α_5 integrin (top) and β_1 integrin (bottom) (n = 3). (**F**) Representative image of insoluble fractions of Triton X-100–fractionated lysates immunoprecipitated for Tie2 and blotted for α_5 integrin.

To further determine the Tie2 dependence of AXT107's effects on EC junctions we used siRNA to knock down Tie2 expression in ECs and then visualized VE-cadherin and actin structures by immunofluorescence. Owing to the poor transfection efficiency of the MECs, we substituted human umbilical vein endothelial cells (HUVECs) for these studies. Treatment with Tie2 siRNA for 48 hours knocked down Tie2 levels in HUVECs by 68% relative to negative control siRNA (Supplemental Figure 5B). We then used immunofluorescence to investigate how Tie2 knockdown influences AXT107-mediated effects on cell junctions (Figure 5C). To provide quantification of the effects we developed a simple metric of VE-cadherin arrangement by comparing the ratios of the true perimeter of the VE-cadherin signal to the apparent minimal junction of the cells (Figure 5D and Supplemental Figure 5C). Confluent monolayers of HUVECs were treated for 48 hours with either Tie2 or negative control siRNA followed by 3 hours with 200 ng/ml Ang2 and either DMSO vehicle or 100 μM AXT107. Consistent with the MEC data in Figure 4A, VE-cadherin in monolayers treated with negative control siRNA exhibited a jagged arrangement in the presence of DMSO but became smoother following treatment with 100 μM AXT107. Knockdown of Tie2 caused a slight, but insignificant, decrease in the jagged appearance of DMSO-treated cells relative to the DMSO-treated cells with negative control siRNA. Most interestingly, however, cells treated with both AXT107 and Tie2 siRNA were significantly more jagged than cells treated with AXT107 and negative control siRNA.

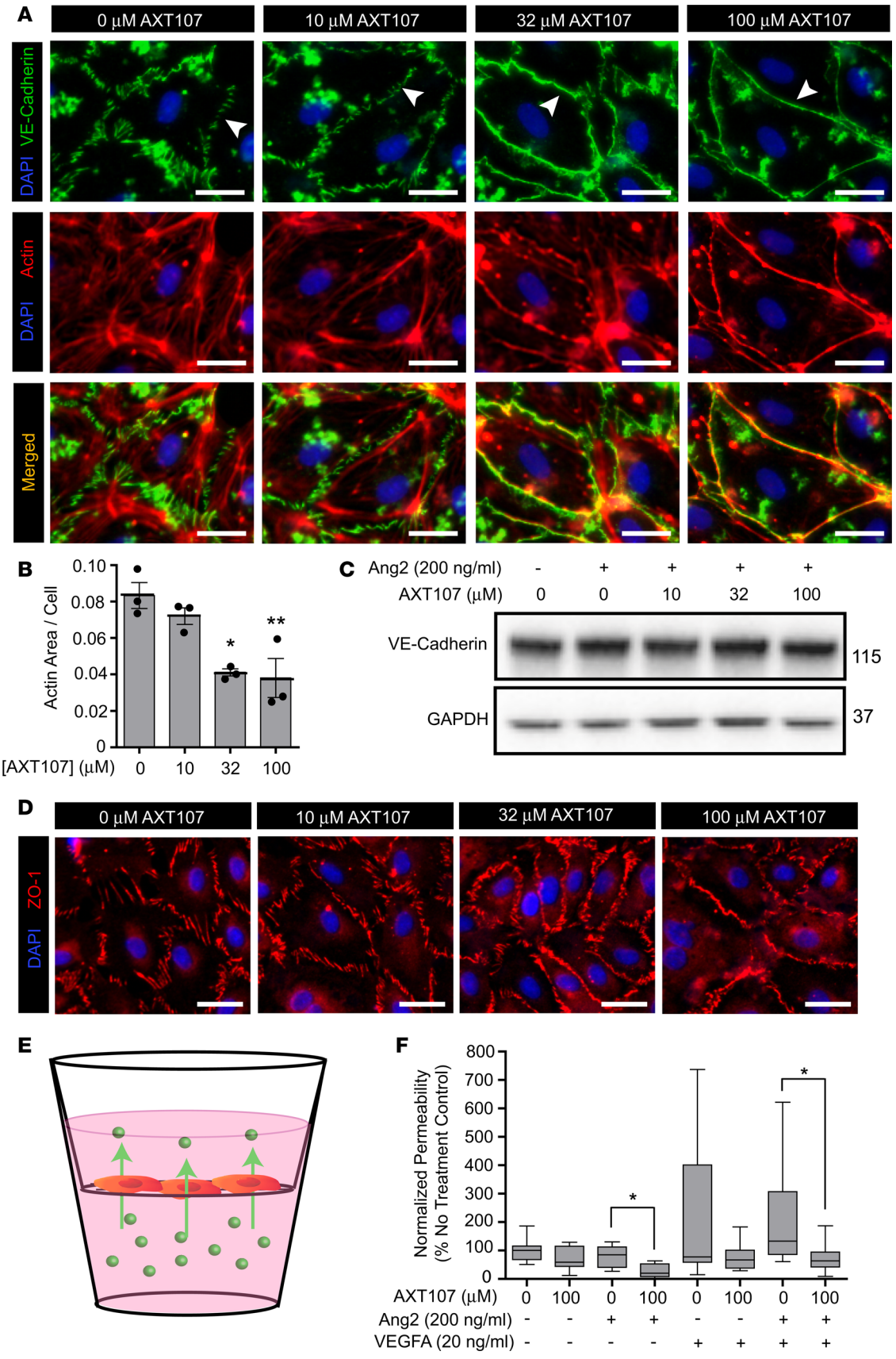
A
0 μM AXT107
10 μM AXT107
32 μM AXT107
100 μM AXT107
DAPI VE-Cadherin
DAPI Actin
Merged
B
Actin Area / Cell
0.10
0.08
0.06
0.04
0.02
0
*
**
[AXT107] (μM) 0 10 32 100
C
Ang2 (200 ng/ml) - + + + +
AXT107 (μM) 0 0 10 32 100
VE-Cadherin
115
GAPDH
37
D
0 μM AXT107
10 μM AXT107
32 μM AXT107
100 μM AXT107
DAPI ZO-1
E
F
Normalized Permeability
(% No Treatment Control)
800
700
600
500
400
300
200
100
0
*
*
AXT107 (μM) 0 100 0 100 0 100 0 100
Ang2 (200 ng/ml) - - + + - - + +
VEGFA (20 ng/ml) - - - - + + + +

Figure 4. AXT107 treatment strengthens endothelial cell junctions. (**A**) Immunofluorescence images of MEC monolayers treated with 200 ng/ml Ang2 and various concentrations of AXT107 that have been stained with DAPI (blue) and antibodies against VE-cadherin (green) and F-actin (red); merged regions are shown in yellow. Arrows indicate representative regions showing transition of VE-cadherin distribution ($n = 3$). Scale bars: 25 μm. (**B**) Average area of F-actin coverage per cell ($n = 3$). $^*P < 0.05$, $^{**}P < 0.01$ by 1-way ANOVA relative to Ang2-alone control. (**C**) Representative Western blots of VE-cadherin from MEC monolayers treated with 200 ng/ml Ang2 for 3 hours and various concentrations of AXT107. GAPDH is included as a loading control. (**D**) Immunofluorescence images prepared as in **A** and stained with DAPI (blue) and an antibody against ZO-1 (red). Scale bars: 25 μm. (**E**) Schematic of the transendothelial permeability assay. (**F**) Quantification of FITC-dextran (40 kDa) migration across MEC monolayers plated on semipermeable substrates following treatment with growth factors and AXT107 where indicated ($n \geq 7$). $^*P < 0.05$ by Student's 2-tailed t test.

AXT107 potentiates Tie2 phosphorylation and stabilizes retinal vasculature in vivo. To investigate the effects of AXT107 on Tie2 activation in vivo we utilized the oxygen-induced ischemic retinopathy (OIR) mouse model. In this model, mouse pups are placed in 75% O_2 at P7 for 5 days, which downregulates VEGF expression and causes regression of newly developed retinal vessels. When the mice are returned to room air at P12 the areas of avascular retina become hypoxic, resulting in stabilization of HIF-1 and an increase in hypoxia-regulated gene products including VEGF and Ang2 (23). This stimulates the growth of retinal neovascularization on the surface of the retina, which is quite extensive at P17. At P17, mice were given an intravitreous injection of 1 μg of AXT107 or vehicle and euthanized 12 hours later (Figure 6A). We used a 12-hour time point, as this duration of treatment is not sufficient to induce major changes in vessel structure, limiting any observations to changes in signaling alone. Such treatment is distinct from our prior investigations in which retinal neovascularization was inhibited following 5 days of AXT107 exposure in the same model (19). Retinas were then dissected and stained with anti–phospho-Tie2 and with *Griffonia simplicifolia* agglutinin (GSA) lectin, which selectively stains ECs. Since GSA lectin more avidly binds activated ECs that are participating in neovascularization than normal ECs, a brief incubation with GSA selectively stains neovascularization, which appears as green tufts on the surface of the retina (Figure 6, B and C, left column). In eyes that had been treated with AXT107, there was robust phosphorylation of Tie2 in ECs participating in neovascularization, but not those in control eyes that had been injected with vehicle (Figure 6B, second and third columns).

Having demonstrated that AXT107 is able to potentiate Tie2 phosphorylation in vivo, we next investigated if it could inhibit retinal vascular permeability in an Ang2 overexpression model. To investigate this we used transgenic IRBP-rtTA/TRE-Ang2 mice, which exhibit doxycycline-induced expression of Ang2 in retinal photoreceptor cells (Supplemental Figure 6A) (24). Vascular leakage was then visualized by fluorescein angiography or quantified by measuring the level of serum albumin in the vitreous. For both experiments mice received intravitreous injections of 1 μg AXT107 in one eye and PBS in the fellow eye. Doxycycline was then administered for 4 days in the drinking water. A schematic of the model can be found in Supplemental Figure 6A. Fluorescence angiography clearly showed Ang2-overexpression-induced fluorescein extravasation from dilated retinal vessels in PBS-injected control eyes (Figure 7A). In contrast, Ang2-overexpressing mice treated with AXT107 showed slightly dilated retinal vessels (Figure 7B) compared with those in untreated, control C57BL/6 mice in which there was no overexpression of Ang2 (Figure 7C). However, like the vessels in control C57BL/6 mice, those in AXT107-injected Ang2 overexpressors had sharp, distinct borders indicating lack of fluorescein leakage through the vessel wall (Figure 7B). Compared with PBS-injected eyes with induced overexpression of Ang2, AXT107-injected eyes with induced overexpression of Ang2 had significantly lower mean levels of serum albumin in vitreous samples (Figure 7D), confirming that AXT107 suppresses Ang2-induced retinal vascular leakage.

AXT107 inhibits vessel permeability in an LPS-induced model of uveitis. Several recent studies have highlighted the contribution of high systemic levels of Ang2 to the severe vascular leakage associated with systemic inflammatory conditions, notably sepsis (25–28). Similarly, a chronic inflammatory condition within the eye, known as uveitis, is associated with excessive vascular leakage and accounts for 10% of blindness worldwide in working-age adults, with higher incidence in developed countries (4). Current treatments for uveitis are the long-term use of corticosteroids and the recently approved systemic anti-TNF antibody Humira (adalimumab), which can be accompanied by severe side effects. Injection of LPS into the vitreous of mice causes severe intraocular inflammation and vascular leakage and is an established model of uveitis (29) (Supplemental Figure 6, B–D). There was a significant increase in retinal Ang2 mRNA levels compared with control, PBS-injected eyes (Figure 7E). Thus, analogous to the situation in sepsis, severe inflammation in the eye is associated with high levels of Ang2 that might contribute to vascular leakage. Pretreatment of LPS-injected eyes with 1 μg of AXT107 resulted in a

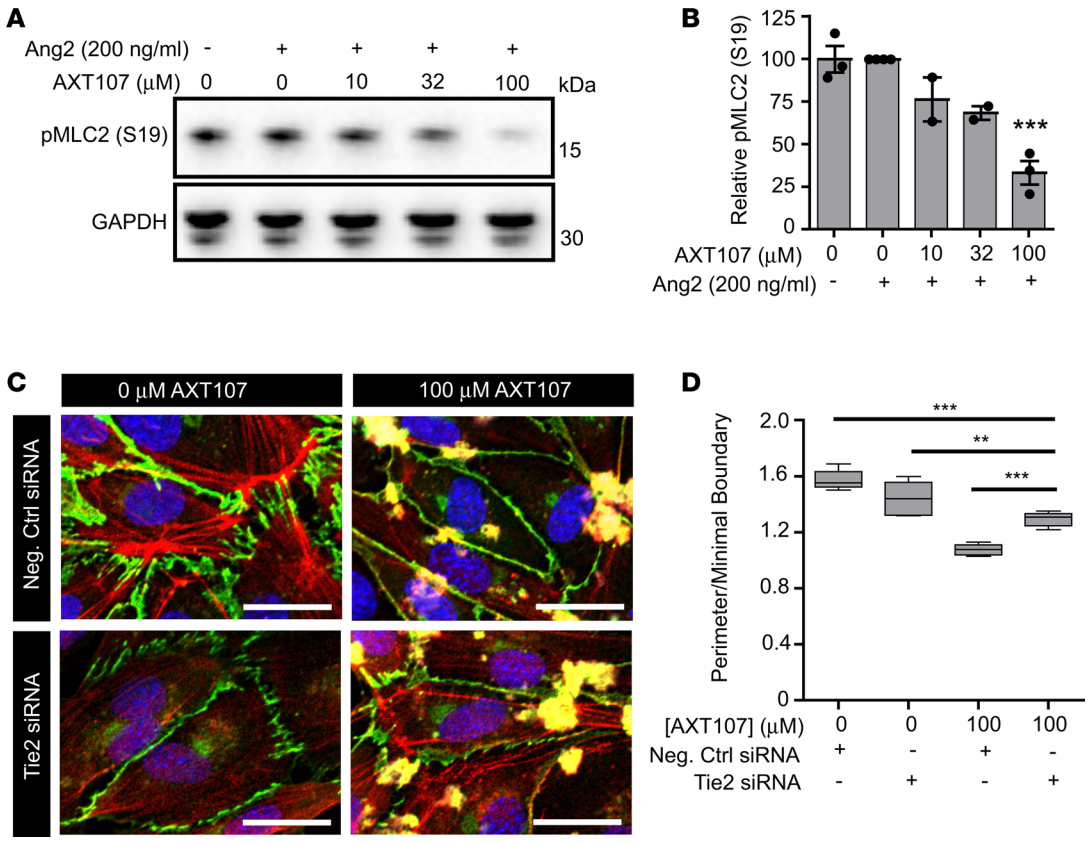

Figure 5. AXT107 influences cell-cell junctions through Tie2-associated mechanisms. (**A**) Representative Western blot images of lysates from MECs treated with 200 ng/ml Ang2 and various concentrations of AXT107 targeting phospho-MLC2, with GAPDH as a loading control. (**B**) Densitometric analysis of images in **A** (n = 2 or 3). ***P < 0.001 by 1-way ANOVA relative to Ang2-alone control. (**C**) Representative immunofluorescence images of HUVEC monolayers treated with 200 ng/ml Ang2, negative control, or Tie2 siRNA, and DMSO or AXT107 that have been stained with DAPI (blue) and antibodies against VE-cadherin (green) and F-actin (red). Scale bars: 25 μm. (**D**) Ratios of actual perimeters to minimal perimeters for images related to **C**. Ratios presented as averages from at least 3 cells from 3 different wells and 2 separate experiments (total of 5 values). ***P < 0.001 by 2-tailed Student's t test.

significant reduction in mean vitreous albumin levels compared with pretreatment with PBS (Figure 7F). Thus, AXT107 suppresses vascular leakage in the setting of severe intraocular inflammation.

Discussion

In this study, we have utilized the unique mechanism of the integrin-binding peptide AXT107 to unveil insights into the regulation of Tie2 signaling by $\alpha_5\beta_1$ integrin. Integrins are well documented to regulate signaling by multiple growth factor receptors, including VEGFR2, c-Met, IGF1R, PDGFRβ, and Tie2. However, the details of these associations have been incompletely understood. Interactions between $\alpha_5\beta_1$ or $\alpha_v\beta_3$ integrins and growth factor receptors potentiate the activation of several receptor tyrosine kinases (RTKs) (30–33) and regulate their internalization (34, 35). Consistent with these findings, integrin inhibition by AXT107 significantly decreased receptor phosphorylation and downstream signals for many of these RTKs (e.g., VEGFR2, c-Met, and IGF1R) as well as reduced total receptor levels through increased receptor degradation (18, 19, 36). In contrast, AXT107 clearly enhances the activation of Tie2 by Ang2 both in vitro and in vivo without altering the total levels of Tie2, suggesting that increased degradation of the receptor was not occurring, as it on exposure to other RTKs.

Our proposed model for Tie2 activation by AXT107 is presented in Figure 8. Specifically, AXT107 stimulates the cell-surface redistribution of Tie2, independent of growth factor treatment. Our data imply that interactions with $\alpha_5\beta_1$ integrin heterodimers sequester Tie2 at the EC-ECM interface. However, since Tie2 does not interact with β_1 integrin in the absence of the α_5 subunit (17), the disruption of these integrins by AXT107 allows for the formation of Tie2-containing complexes at EC-EC junctions. This junctional relocation appears to be important for activation, as both our immunofluorescence and pull-down experiments suggest that phosphorylation

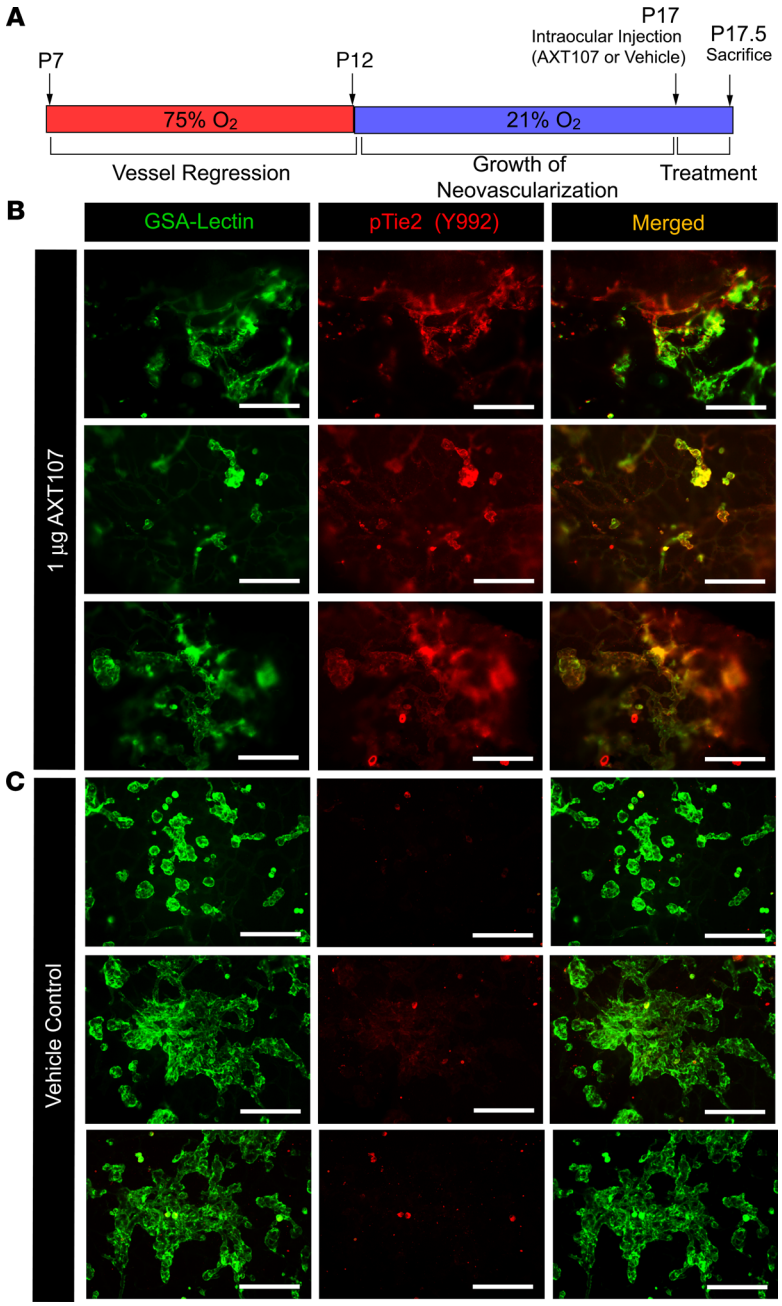

Figure 6. AXT107 potentiates Tie2 phosphorylation in vivo. (**A**) Schematic depicting each step in the OIR model, with oxygen concentration and injection times indicated. (**B** and **C**) Immunofluorescence images of retinas from mouse OIR models treated with 1 μg AXT107 (**B**) or DMSO vehicle (**C**). AXT107 was delivered by intraocular injection 5 days after removing mice from hyperoxia. Retinas were excised and briefly incubated with FITC-GSA lectin (green) to selectively stain endothelial cells participating in neovascularization and also stained for phopsho-Tie2 (red). Scale bars: 200 μm.

is limited to the junctions. A potential mechanism for how this relocation could activate Tie2 may be related to the natural differences between Ang1 and Ang2. Previous reports have suggested that the superior activation of Tie2 by Ang1 versus Ang2 is a result of its ability to form larger complexes than Ang2 and induce the formation of Tie2 clusters (37, 38). Since total cellular levels of Tie2 did not change with AXT107, the increase in junctional Tie2 would imply an elevation in receptor concentration within these regions of the cell. Additionally, the coimmunoprecipitation assays in Figure 2B and Supplemental Figure 3B consistently showed greater pull-down of Tie2 in AXT107-treated lysates despite the use of equal volumes throughout the lysing process, suggesting that Tie2 had formed clusters in these samples. Together, these data suggest that AXT107 both relocates Tie2

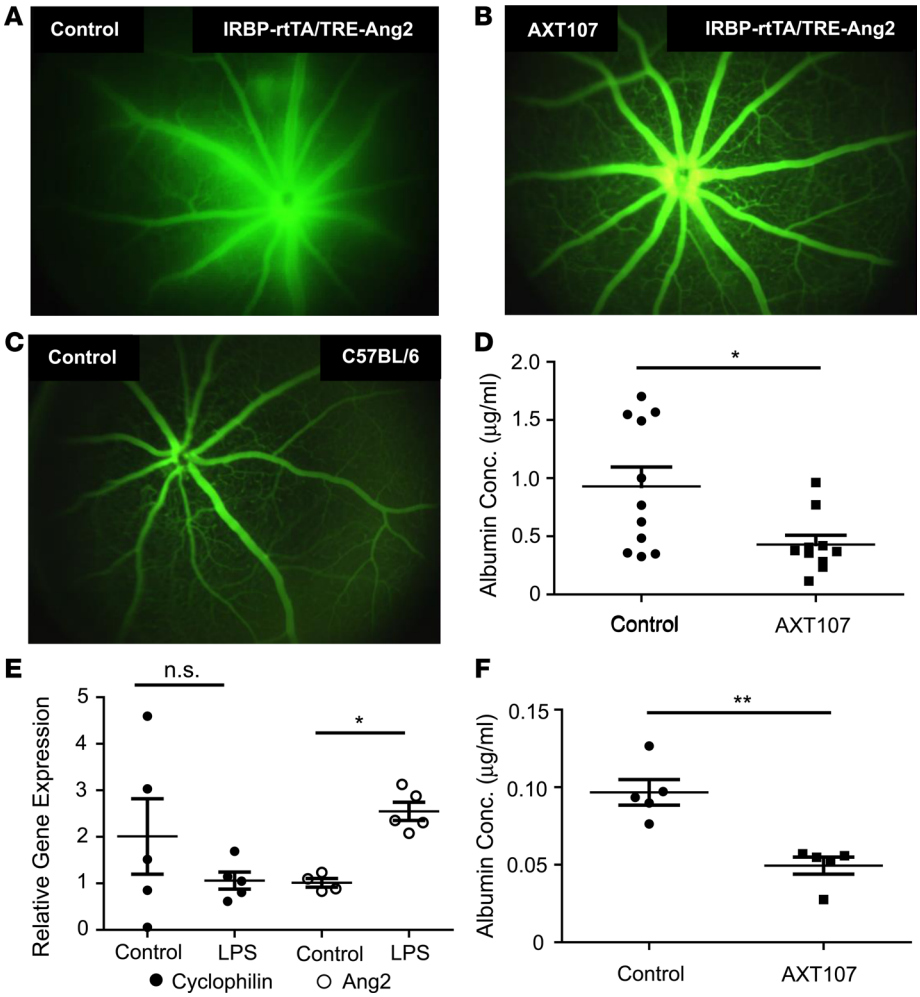

Figure 7. AXT107 inhibits Ang2- and LPS-mediated vascular permeability in the mouse eye. (**A**–**C**) Representative fluorescein angiography images of mouse eyes from IRBP-rtTA/TRE-Ang2 mice with doxycycline-induced overexpression of Ang 2 in the retina given an intravitreous injection of PBS (**A**) or 1 μg of AXT107 (**B**). Compared with the normal retinal vessels seen in an untreated wild-type C57BL/6 mouse, the Ang2-overexpressing PBS-injected control shows dilated retinal vessels with extravasation of fluorescein blurring the margins of the vessels (**A**), while the AXT107-treated Ang2 overexpressor shows sharp vessel margins, indicating no fluorescein leakage and mild vasodilation (**B**). (**D**) Doxycycline-treated IRBP-rtTA/TRE-Ang2 mice given an intravitreous injection of 1 μg of AXT107 had a significant reduction in mean level of albumin in the vitreous compared with PBS-injected controls; $n = 11$; $P < 0.05$ by Mann-Whitney test. (**E**) Relative gene expression of cyclophilin and Ang2 in the retinas of mice treated with intravitreous injection of 125 ng LPS or PBS control. Fold changes were determined by ΔΔCT ($n = 4$ or 5). $P < 0.01$ by Mann-Whitney test. (**F**) Mean vitreous albumin level in mice with LPS-induced uveitis was significantly less in those given an intravitreous injection of 1 μg AXT107 compared with PBS-injected controls ($n = 5$). $P < 0.01$ by Mann-Whitney test.

to the junctions and stimulates its clustering. Phosphorylation of these complexes, however, still requires the angiopoietins (Supplemental Figure 1C). Precluding the need for clustering, AXT107 potentiates Tie2's activation by Ang2. In contrast, Ang1, which already possesses this characteristic, is minimally affected. In fact, at the highest concentration, AXT107 slightly inhibited Ang1-induced Tie2 phosphorylation (Figure 1A), suggesting that the clusters formed by both molecules may differ slightly. The effects of AXT107 on Tie2 phosphorylation do not appear to be the result of VE-PTP inhibition, such as that observed with AKB-9778 (22), as no change in VE-PTP interactions were observed in peptide-treated samples. However, it is possible that the formation of clustered Tie2 complexes at the junction could spatially limit the access of VE-PTP to some Tie2 receptors. The Tie2 coreceptor Tie1 was also found within the junctional Tie2 complexes, suggesting that the peptide does not disrupt these interactions and, thus, does not conflict with the recent observation that activation of Tie2 at the junctions is dependent on Tie1 (16, 21). These data do not indicate whether AXT107 directly stimulates the relocation of Tie1 to the EC junctions or if Tie1 is indirectly relocated through interactions with Tie2.

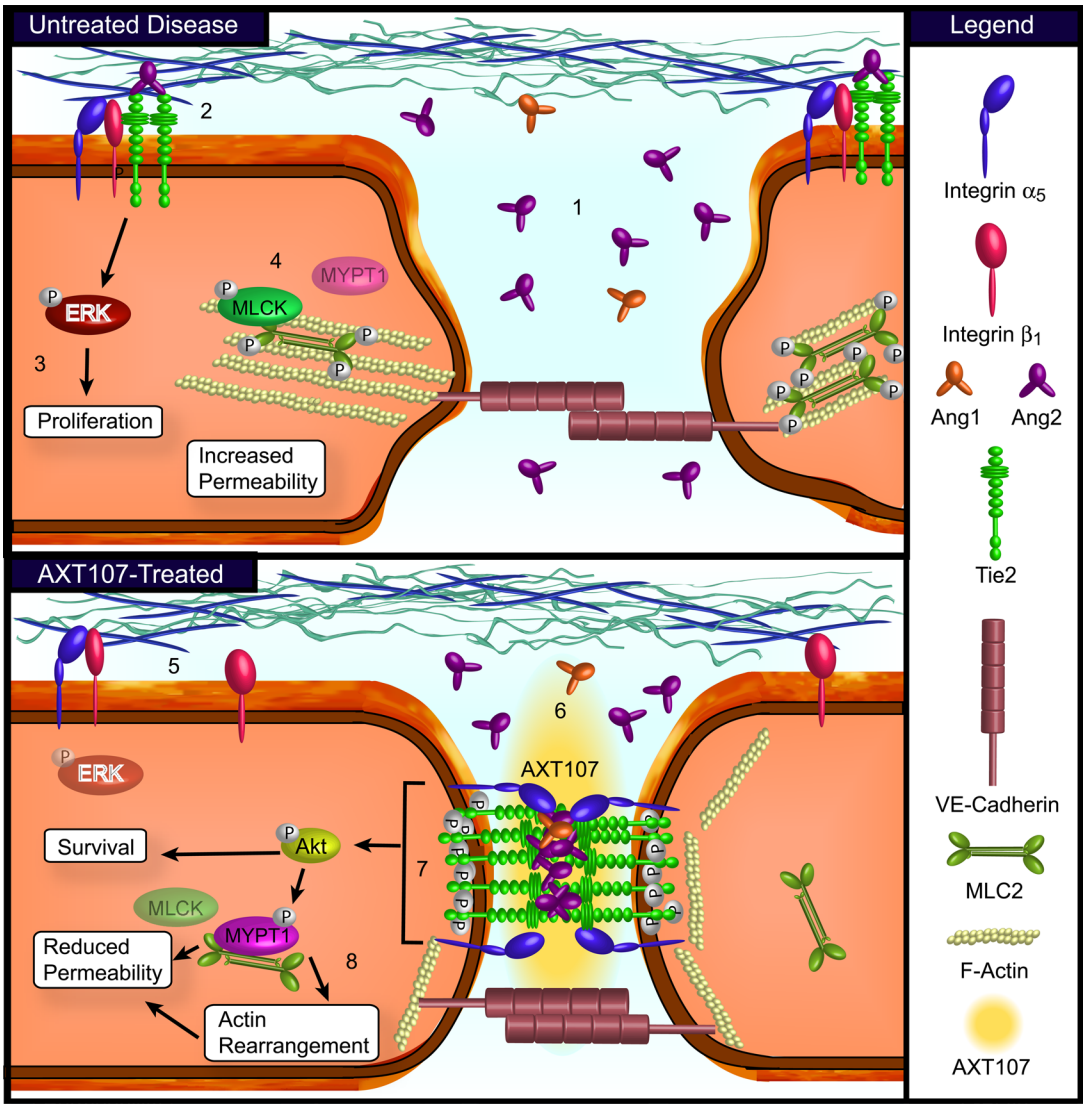

Figure 8. Model for AXT107-mediated activation of Tie2. Top: In diseased neovasculature (1) the lack of pericyte coverage skews the ratio of angiopoietins towards Ang2, which (2) weakly activates Tie2 in complex with integrin $\alpha_5\beta_1$ heterodimers at the cell-ECM interface, (3) preferentially activating proliferative signals (i.e., ERK1/2). (4) The MLC kinase (MLCK) phosphorylates MLC2 and leads to formation of radial actin stress fibers within the cell and tension at EC-EC junctions. Bottom: In the presence of AXT107 (5) a fraction of α_5 integrin separates from β_1 integrin and (6) migrates to EC-EC junctions along with Tie2 to form large complexes and trans-interactions across junctions. (7) These complexes potentiate the phosphorylation of Tie2 by Ang2, thereby activating Akt-mediated survival pathways while maintaining basal levels of phospho-ERK1/2. (8) Additionally, MLC phosphatase is activated via the RAP1 or RAC1 pathway, which leads to reduced MLC2 activity, increased cortical actin, and stabilized junctions.

Our findings regarding the Tie2-integrin relationship fit with many previous observations reported in other studies. When Tie2 is associated with integrins, Ang1 preferentially activates downstream signals related to proliferation (e.g., the ERK1/2 pathway) and migration (e.g., FAK and Dok-R) relative to survival responses (e.g., Akt) (8, 10, 17, 20). Notably, Tie2-dependent proliferation and migration of sparsely cultured or newly attached ECs were particularly sensitive to $\alpha_5\beta_1$ integrin interactions. In contrast, the loss of α_5 integrin by siRNA was previously shown to shift signaling from the ERK1/2 pathway to the Akt-mediated prosurvival response (10). Similarly, our studies, which focused on confluent EC monolayers, demonstrate a clear Ang2-mediated activation of Akt following integrin inhibition by AXT107 without a comparable change in ERK1/2 phosphorylation. Surprisingly, the knockdown of β_1 integrin has been previously shown to decrease Akt phosphorylation, which contrasts with the results from α_5 integrin knockdown and our results with AXT107 treatment (16). As a possible explanation, β_1 is the most promiscuous partner of α integrins and decreases in its protein levels may impact more cellular activities, both Tie2-dependent and -independent, in comparison with the knockdown of the relatively specific α_5 integrin or conditions in

which integrin levels remain constant but are inhibited. In particular, AXT107 only disrupted about half of the $\alpha_5\beta_1$ integrin heterodimers according to our Duolink assay and many of the α_5 and β_1 integrin subunits within the Triton X-100–soluble fractions remained associated even in the presence of peptide, as shown by our immunoprecipitation data. Alternatively, β_1 integrin may be essential for the initial formation of Tie2 signaling complexes but may be dispensable once they are formed. Taken together, these findings emphasize the importance of integrins in the preferential activation of signaling pathways downstream of Tie2.

The roles of integrin interactions in the regulation of Tie2 signaling suggest that natural mechanisms may exist to separate α_5 and β_1 integrins within the cell. The treatment of ECs with COMP-Ang1 has been previously shown to induce junctional relocation of Tie2 in ECs and transfected HeLa cells (20, 39), which may suggest that the angiopoietin ligands are able to stimulate this activity under specific conditions. This hypothesis is not unprecedented, as a recent report has shown that cMet can displace α_5 integrin and associate with β_1 integrin under certain conditions (40). In contrast, β1 integrin did not relocate to the junctions in Tie2-transfected HeLa cells in response to treatment with either Ang1 or Ang2 (39). While we can only speculate as to the mechanism of this dissociation, earlier reports have shown that the activities of both Ang1 and $\alpha_5\beta_1$ integrin are dependent on glycosylation. Specifically, the mutation of several N-glycosylated sites on either the β-propeller of α_5 integrin or the I-like domain of β_1 integrin disrupted heterodimerization of the proteins and their interactions with FN1 (41, 42). Likewise, both Ang1 and Ang2 are glycoproteins and interact directly with integrins (10, 43). Therefore, AXT107 or angiopoietins may disrupt the glycan interactions between α_5 and β_1 integrins and cause them to dissociate.

The $\alpha_5\beta_1$ integrin heterodimers that were disrupted by AXT107 represented about half of the population and only a small fraction was found to relocate to the junctions. The factors determining the susceptibility of integrin heterodimers to this effect remain undetermined. Given the AXT107-mediated rearrangement of Tie2 to the junctions and the continuation of interactions between the receptor and the α_5 integrin subunit, it may be that the varying composition of integrin complexes (e.g., RTK association) may influence their susceptibility to disruption. Integrins are known to adopt various conformations that regulate their functions in response to ligand and adaptor protein binding (reviewed in ref. 44). For instance, VEGFR2 has been found to interact specifically with the extended, or activated, $\alpha_v\beta_3$ integrin complexes associated with ECM ligands (45). Of particular interest, Tie2 interactions with $\alpha_5\beta_1$ integrins are stabilized in the presence of FN1, suggesting that Tie2 preferentially interacts with extended conformations of $\alpha_5\beta_1$ integrins as well (10, 17). While there is currently not enough evidence to conclusively state that AXT107 preferentially interacts with specific integrin complexes or conformations, these data do emphasize the variability in integrin structures that could contribute to our experimental observations.

The antipermeability properties of AXT107 have been previously demonstrated in animal models of the eye; however, the mechanistic details were unknown (19). The above data provide strong evidence that this effect, at least in part, is due to the potentiation of Tie2 signaling and are consistent with other results found in the Tie2 literature. Notably, AXT107 was able to block the vascular leakage associated with overexpression of Ang2 and knockdown of Tie2 by siRNA reduced the rearrangement of VE-cadherin following peptide treatment. Similar findings were shown in other studies in which siRNA-mediated knockdown of Tie2 was found to increase the permeability of EC monolayers and was associated with the presence of radial actin (9, 39). Conversely, the activation of Tie2 by the VE-PTP inhibitor AKB-9778 was found to stabilize cell-cell junctions similarly to AXT107 by rearranging actin distribution from radial to cortical and, consequently, changing VE-cadherin distribution from jagged to smooth and decreasing monolayer permeability (9). Likewise, both AXT107 and AKB-9778 treatments are associated with a decrease in the phosphorylation of MLC2, an effect that has been connected to the activities of the Rap1 and Rac1 GTPases. Moreover, the antipermeability properties of AXT107 specifically benefit from the peptide's ability to inhibit the signaling of other RTKs, notably VEGFR2. As demonstrated in our Transwell permeability assay, AXT107 alone was able to inhibit VEGFA-induced permeability across the endothelial monolayer and this effect could be enhanced in the presence of Ang2. Together, these data emphasize the therapeutic potential of inhibiting the VEGFR2 pathway and activating Tie2 signaling simultaneously using AXT107 as a therapeutic to counter excessive vessel permeability.

Perturbations in Ang/Tie signaling are well documented in several diseases associated with vascular permeability, blood and lymphatic vessel development, and inflammatory/immune responses (reviewed in ref. 46). Recently, EC knockdown of Tie1 was found to stabilize tumor vasculature by activating Ang1/Tie2 signaling, which consequently improved pericyte coverage and vessel perfusion and decreased metastasis and late-stage

tumor growth (47). Furthermore, elevation of serum Ang2 levels is of prognostic value in certain cancers and has been correlated with tumor progression, angiogenesis, metastasis, and patient survival. Likewise, a high serum Ang2-to-Ang1 ratio in sepsis is associated with an increased disease severity and a poor prognosis resulting from vessel hyperpermeability (27, 28). Recently, potentially deadly thrombotic complications in sepsis have been associated with decreased Tie2 phosphorylation stemming from the high Ang2 concentrations in the disease (26). While neutralization of Ang2 by antibody treatment was found to maintain vessel stability and improve survival in mouse models of sepsis (28), our data suggest that this abundance of Ang2 in these conditions can be used to activate beneficial Tie2 signaling. Moreover, our results extend these observations to the eye and implicate the possibility of the Ang2/Tie2 pathway as a new treatment target in uveitis. Similarly to the increase in systemic Ang2 levels in sepsis models, there was an increase in Ang2 levels in the retina in LPS-induced uveitis and the activation of Tie2 by Ang2 in the presence of AXT107 may contribute to the antipermeability effect of AXT107 in this uveitis model. Studies using an Ang2-clustering antibody, ABTAA (Ang2-binding and Tie2-activating antibody), support this assertion. Treatment of mouse sepsis models with ABTAA improved the efficacy of treatment beyond that provided by an Ang2-neutralizing antibody by also activating the Tie2 receptor (25). In tumors, the activation of Tie2 by ABTAA has also been shown to improve the effects of chemotherapy by normalizing tumor vasculature and improving drug delivery (48). Similar to ABTAA, AXT107 altered Ang2 to behave more like Ang1 by facilitating Tie2 activation instead of simply blocking its activity.

In eyes with ischemic retinopathy, increased levels of Ang2 contribute to vascular leakage and macular edema (15). Phase 2 clinical trials have shown that inhibitors of Ang2 combined with VEGF suppression using ligand-neutralizing antibodies provide greater benefit than VEGF suppression alone in patients with diabetic macular edema. Clinical trials to test if these results versus ranibizumab also hold for NVAMD are ongoing. By converting Ang2 from an antagonist of Ang1-mediated activation of Tie2 to a Tie2 agonist, AXT107 takes advantage of the elevated levels of Ang2 in these disease states. Importantly, the mechanism through which AXT107 activates Tie2 is both complementary to and independent from that of the low endogenous levels of Ang1 and does not suffer from the incomplete inhibition of antibodies that target Ang2-like ligands. Moreover, we have previously demonstrated that AXT107 blocks signaling through VEGFR2 and other angiogenic receptor tyrosine kinases, with longer duration of action via the formation of a self-assembled clear-gel depot that serves as a sustained delivery reservoir (19). This unique combination of properties demonstrated by AXT107 may provide improved and longer-lasting benefits when compared with standard anti-VEGF monotherapies and may be developed as a new therapy for highly prevalent retinal and choroidal vascular diseases.

Methods

Cell culture and reagents. Human dermal MECs (Lonza) were maintained at 37°C and 5% CO_2 in EBM-2MV media (Lonza) and used from passages 2 through 7. Where applicable, cells were serum starved in EBM-2 media (Lonza) with no supplements. For FITC-dextran permeability assays, phenol red–free media were used to avoid autofluorescence. AXT107 was manufactured at New England Peptide by solid-state synthesis, lyophilized, and dissolved in 100% DMSO. After dilution, DMSO concentrations never exceeded 0.25% in any experiment.

Western blotting. For Ang1/2 signaling investigations, cell culture dishes (10 cm diameter) were coated with 5 μg/ml FN1 (Sigma-Aldrich) for 2 hours at 37°C. The FN1 solution was then removed by aspiration and 5×10^6 MECs were plated in EGM-2MV media and cultured for 48 hours at 37°C. The cells were then serum starved for 16 hours in serum-free EGM-2 base media. AXT107 (0–100 μM as indicated) was subsequently added to each culture and incubated for 75 minutes at 37°C. The cultures were then treated with 1 mM sodium vanadate (New England Biolabs) for 15 minutes followed by stimulation with 200 ng/ml angiopoietin (R&D Systems) for an additional 15 minutes. The cells were then transferred to ice, washed twice with ice-cold Dulbecco's PBS (DPBS) containing Ca^{2+} and Mg^{2+}, and collected by scraping in 500 μl of 1× Blue Loading Buffer (Cell Signaling Technology). Lysate samples were then sonicated, boiled, and resolved by SDS-PAGE. Specific proteins were identified by Western blot, using the following primary antibodies: phospho-Tie2 (Y992) (catalog 4221), Tie2 (catalog 7403), phospho-Akt (S473) (catalog 4058), Akt (catalog 9272), phospho-p44/42 MAPK (ERK1/2; T202/Y204) (catalog 4370), p44/42 MAPK (ERK1/2) (catalog 4695), β_1 integrin (catalog 34971) (all Cell Signaling Technology); β_1 integrin (catalog 610467, BD Transduction Laboratories); and α_5 integrin (catalog AB1928, Millipore) and detected with HRP-conjugated goat anti-rabbit and sheep anti-mouse secondary antibodies (GE Healthcare).

Triton X-100 fractionation. The isolation of Triton X-100–soluble and –insoluble fractions was performed using modifications to previously described procedures (49). FN1-coated 6-well plates were seeded with 2.5×10^6 cells and cultured for 48 hours as described above. The cultures were then serum starved for 90 minutes in EBM-2 media, treated with 100 μM AXT107 or DMSO vehicle, and treated for 15 minutes with 1 mM sodium vanadate. The cells were then stimulated with 100 ng/ml VEGFA, 400 ng/ml Ang2, or PBS for 15 minutes. The plates were then transferred to ice and washed twice with cold DPBS containing Ca^{2+} and Mg^{2+} and twice with EBM-2 media. The media were then removed and the cells incubated for 30 minutes on ice at 4°C in 200 μl of Triton X-100 extraction buffer (10 mM Tris-HCl, pH 7.5; 150 mM NaCl, 2 mM $CaCl_2$, 1% NP-40, 1% Triton X-100, and a protease inhibitor cocktail [Cell Signaling Technology, catalog 5871]) with occasional agitation. The extraction buffer was gently collected and centrifuged at 12,000 *g* for 5 minutes. The supernatant was then mixed with 125 μl of 3× Blue Loading Buffer, boiled, and saved as the Triton X-100–soluble fraction at –20°C. The remaining insoluble fraction was washed twice with wash buffer (10 mM Tris-HCl, pH 7.5; 150 mM NaCl, Complete Mini protease inhibitor tablets [Roche]) and collected in 375 μl of 1× Blue Loading Buffer with scraping followed by centrifugation and boiling as described above. This lysate was saved at –20°C as the Triton X-100–insoluble fraction. Samples were analyzed by Western blot as described above.

For pull-down variations, insoluble fractions were instead collected in RIPA buffer (Sigma-Aldrich) supplemented with a protease and phosphatase inhibitor cocktail (Cell Signaling Technology) and 5 mM EDTA. Lysates were sonicated briefly and incubated for 1 hour with anti-Tie2 (Cell Signaling Technology, catalog 4224) or anti–α_5 integrin (Millipore, catalog AB1928) with end-over-end mixing. Subsequently, 20 μl of Protein Agarose A/G beads (Santa Cruz Biotechnology) was added and the samples incubated for another hour. Beads were collected by centrifugation at 1,500 *g* and 4°C, washed 4 times with PBS, resuspended in SDS-based Blue Loading Buffer, boiled, and resolved by SDS-PAGE.

Immunofluorescence. Black, clear-bottom, 96-well plates with half well size were coated with 10 μg/ml FN1 for 2 hours at 37°C. The FN1 solution was then removed by aspiration and the plate seeded with 4×10^3 MECs in EGM-2MV media. After 24 hours, the cells were washed once with DPBS containing Ca^{2+} and Mg^{2+} to remove dead cells and then the cells allowed to grow for an additional 24 hours. For 3-hour-duration treatments (i.e., VE-cadherin), cells were washed twice with DPBS containing Ca^{2+} and Mg^{2+} and serum starved in EBM-2 for 3 hours. The media were then removed and the cells treated with 100 μl of EBM-2 media containing 200 ng/ml Ang2 or PBS and varying concentrations of AXT107 or DMSO for 3 hours. For 15-minute-treated samples (i.e., phospho-Tie2), the cells were serum starved in EBM-2 media for 165 minutes, incubated for 90 minutes with varying concentrations of AXT107 or DMSO in EBM-2, and finally stimulated for 15 minutes with 200 ng/ml Ang2 or PBS supplemented with peptide to retain the same concentrations. These times were chosen so that both treatment procedures would be completed at the same time. The cells were then washed twice with cold DPBS containing Ca^{2+} and Mg^{2+} and fixed in 10% neutral buffered formalin for 15 minutes. The formalin solution was then removed, and the wells were washed 3 times in DPBS containing Ca^{2+} and Mg^{2+}. The cells were then blocked in blocking buffer (5% normal goat serum, 0.3% Triton X-100 in DPBS containing Ca^{2+} and Mg^{2+}) and stained for 16 hours with primary antibodies against phospho-Tie2 (Y992) (R&D Systems, catalog AF2720), total Tie2 (Genetex, catalog GTX107505), VE-cadherin (Cell Signaling Technology, catalog 2500), or ZO-1 (ThermoFisher Scientific, catalog 33-9100) diluted 1:150 in antibody dilution buffer (1% BSA; 0.3% Triton X-100 in DPBS containing Ca^{2+} and Mg^{2+}). The wells were then washed 3 times with DPBS and incubated for 1 hour with Alexa Fluor 488–conjugated goat anti-rabbit secondary antibodies (Cell Signaling Technology, catalog 4412) diluted 1:300 in antibody dilution buffer. The wells were then washed twice and stained with Alexa Fluor 555–conjugated phalloidin (Cell Signaling Technology, catalog 8953) diluted 1:20 in PBS for 20 minutes. The cells were then washed twice again in DPBS, stained with DAPI for 20 minutes, and exchanged for DPBS for imaging. Cells were imaged using the BD Pathway 855 system and Attovision software (BD Biosciences) or the Zeiss Axio Observer with LSM700 confocal module and Zen LE software (Zeiss).

Duolink protein interaction analysis. Black, clear-bottom, 96-well plates were coated with FN1 and seeded with MECs as described for immunofluorescence experiments above. After growing for 48 hours, cells were serum starved for 3 hours, treated with 100 μM AXT107 or DMSO vehicle for 90 minutes, washed 4 times with DPBS containing Ca^{2+} and Mg^{2+}, and fixed in 10% neutral buffered formalin. Cells were blocked in 5% normal goat serum, 0.3% Triton X-100 in DPBS containing Ca^{2+} and Mg^{2+} for 1 hour, and incubated overnight at 4°C with primary antibodies in PBS containing Ca^{2+} and Mg^{2+} with 1% BSA and 0.1% Triton X-100.

Interaction spots were developed using anti-rabbit PLUS and anti-mouse MINUS complementary secondary antibody probes and the Duolink (Sigma-Aldrich) green detection reagent according to the manufacturer's instructions and detected using the BD Pathway 855 system or the Zeiss Axio Observer with LSM700 confocal module.

FITC Transwell permeability assay. Transwell, 24-well inserts (Corning) were coated with 7.5 μg/cm^2 FN1 for 2 hours at 37°C, aspirated, and then dried for 30 minutes at room temperature. Wells were then seeded with 7.5 × 10^4 MECs in 100 μl of EBM-2 media (without phenol red) and allowed to settle for 30 minutes at room temperature. Subsequently, 1 ml of EGM-2 media was added to the bottom chamber, with an additional 200 μl to the top chamber. The plate was incubated for 24 hours at 37°C, after which the media were aspirated as carefully as possible and an additional 7.5 × 10^4 MECs were plated in each well as described above. After 48 hours at 37°C, the media were aspirated from both chambers and the cells were washed twice in DPBS containing Ca^{2+} and Mg^{2+}, once with EBM-2 media (without phenol red), and serum starved in EBM-2 media applied to both chambers for 2 hours at 37°C. After this incubation, 100 μM AXT107 or an equivalent amount of DMSO vehicle was added, and the plates were incubated for an additional 90 minutes. The cells were then treated with 200 ng/ml Ang2, 100 ng/ml VEGFA, both, or PBS control in the top chamber and 25 μg/ml FITC-dextran (40 kDa) in the bottom chamber. AXT107 was also added to both chambers to maintain a concentration of 100 μM. After 3 hours, 10 μl was removed from the top chamber of each well and mixed with 90 μl of water in a clear-bottom, 96-well plate. Fluorescence values for each sample were calculated using a PerkinElmer Victor V fluorescence plate reader.

siRNA knockdown of Tie2 in HUVECs. HUVECs were cultured to confluence in FN1-coated 96-well or 6-well plates as described for the immunofluorescence experiments with MECs above, except that 6-well plates were seeded with 2.5 × 10^5 cells. Once the cells were confluent, the media were exchanged with fresh EGM-2MV media. A transfection solution was prepared using 25 nM Tie2 siRNA or negative control siRNA and the TransIT-TKO reagent (Mirus Bio) according to the standard protocol for the corresponding plate sizes. Solutions were incubated for 30 minutes before their addition to the wells. Cells were incubated with the siRNA for 48 hours and then washed twice with PBS with Ca^{2+} and Mg^{2+}. The following siRNAs were used: negative control, MISSION siRNA Universal Negative Control (Sigma-Aldrich, SIC001); and Tie2, MISSION siRNA, Human kinase TEK (Sigma-Aldrich, SASI_hs01 00185199).

The 6-well plates were used to determine transfection efficiency and were lysed in 120 μl of SDS-loading dye and analyzed by Western blot as described above. The 96-well plates were used for immunofluorescence experiments with and without 100 μM AXT107 treatment using the procedures described above for VE-cadherin and actin staining, starting with the 3-hour serum starvation. Images were taken using the Zeiss Axio Observer with LSM700 confocal module and analysis of the junctions was performed using ImageJ (NIH). VE-cadherin perimeters and minimal cell junction perimeters were traced by hand using the freehand and polygon shape tools respectively as demonstrated in Supplemental Figure 5C. At least 3 cells from each well were analyzed and the ratios of the VE-cadherin perimeters to cell junction perimeters were averaged. At least 3 wells were analyzed per condition over 2 separate experiments.

OIR mouse model and immunofluorescence. OIR experiments were performed similarly to those described previously (22). Retinal ischemia was induced by placing litters of P7 C57BL/6 mouse pups of either sex in 75% ± 3% oxygen. After 5 days, the pups (P12) were returned to room air and neovascularization was allowed to develop for 5 days. At P17, mice were given an intraocular injection of 1 μg AXT107 or an equivalent volume of the 5% DMSO vehicle. After 12 hours, the mice were euthanized and eyes were fixed in 10% PBS-buffered formalin for 10 minutes followed by 3 hours in 4% paraformaldehyde at room temperature. Retinas were dissected and blocked with 8% normal goat serum for 45 minutes. After a brief wash, retinas were stained with rabbit anti-Tie2 (1:200, R&D Systems) at 4°C overnight with rotation. The following day, the retinas were washed an additional 3 times and stained with a goat anti-rabbit IgG conjugated with Alexa Fluor 594 (1:800, Invitrogen) and FITC-conjugated GSA isolectin B4 (1:150, Vector Laboratories) for 45 minutes at room temperature. Images were taken using a Zeiss fluorescence microscope.

Transgenic mouse models. Adult (5–6 weeks old) double-transgenic IRBP-rtTA/TRE-Ang2 mice of either sex were treated with 1 μg of AXT107 in one eye and PBS in the fellow eye. The mice were then given drinking water containing 2 mg/ml doxycycline (Sigma-Aldrich) for 3 days. On day 4 after injection of AXT107 or PBS, vitreous samples were collected to measure the albumin levels using an albumin ELISA kit (ab108791, Abcam).

Fluorescence angiography. Adult (5–6 weeks old) double-transgenic IRBP-rtTA/TRE-Ang2 mice of either sex were treated by intravitreous injection of 1 μg of AXT107 in one eye and PBS in the fellow eye. Untreated C57BL/6 mice were used as normal controls. Four days later, mice were anesthetized with a

mixture of ketamine and xylazine hydrochloride, pupils were dilated with 1% tropicamide, and mice were then perfused with 10% fluorescein sodium (AK-Fluor, Akorn). Images were examined by fluorescence microscopy using a Micron III microscope (Phoenix Research Laboratories, Inc.).

Mouse models of LPS-induced inflammation. For characterization experiments, adult (5–6 weeks old) C57BL/6 mice of either sex were treated with 150 ng LPS for RT-qPCR experiments and 250 ng LPS for vascular permeability experiments in C57BL/6 mice in one eye and PBS in the fellow eye. For RT-qPCR, mice were euthanized after 24 hours, the eyes were enucleated, retinas were dissected free of other ocular tissue, and RNA was isolated from the retinas. The RNA was used to prepare cDNA with an iScript DNA Synthesis Kit (Bio-Rad Laboratories) according to the kit instructions. Real-time quantitative PCR was performed using a Rotor Gene Q instrument (Qiagen) and Rotor-Gene SYBR Green PCR Kit (Qiagen) to investigate the expression levels of Ang2 and IL-6 in the retinas of PBS- and LPS-injected eyes. Cyclophilin A expression was used to standardize expression levels of the test genes. Fold changes in gene expression were calculated using ddCt values (50). The following primers were used in these experiments: Ang2 (51) forward, 5′-CTGTGCGGAAATCTTCAAGTC-3′ and reverse, 5′-TGCCATCTTCTCGGTGTTG-3′; cyclophilin A (52) forward, 5′-CTGTGCGGAAATCTTCAAGTC-3′ and reverse, 5′-TGCCATCTTCTCGGTGTTG-3′; and IL-6 (53) forward, 5′-GAGGATACCACTCCCAACAGACC-3′ and reverse, 5′-AAGTGCATCATCGTTGTTCATACA-3′.

For investigations of the effect of AXT107 on vascular leakage, one eye was injected with 1 μg of AXT107 and the fellow eye with PBS by intravitreous injection. After 24 hours, both eyes received intravitreous injections of 250 ng LPS. After an additional 24 hours, the concentration of serum albumin was then determined for each eye by ELISA as for the transgenic mouse models above.

Statistics. Unless otherwise stated, error bars represent SEM. Statistics were determined by unpaired Student's *t* test (2-tailed), Mann-Whitney test, or ANOVA as indicated in the corresponding figure legends using GraphPad Prism software v. 5.0. A P value less than 0.05 was considered significant. All image analysis was performed with ImageJ.

Study approval. Mice were treated in accordance with the Association for Research in Vision and Ophthalmology Guidelines regarding the care and use of animals in research. All animal studies were approved by the IACUC of Johns Hopkins University.

Author contributions

ACM designed and performed experiments, interpreted the data, made figures, and drafted the manuscript. JS, RLS, and VEL designed and performed experiments, interpreted the data, and made figures. ZC and NCS performed experiments and analyzed data. JJG helped draft the manuscript and interpreted the data. PAC, ASP, and NBP assisted in experimental design, provided funding, interpreted the data, edited the manuscript, and supervised the experimental work.

Acknowledgments

We thank the Johns Hopkins University ChemCore facility for the use of their BD Pathway 855 automated confocal microscope and School of Medicine Microscopy Facility (MicFac) for the use of the Zeiss LSM700 confocal microscope, supported by the Office of the Director of the NIH under the award S10OD016374. This research was supported by NIH grants F32CA210482 (to ACM), R21EY026148, R01CA138264, R43EY025903, R01EY028996, R01HL101200, and R44EY025470, the Research to Prevent Blindness/Dr. H. James and Carole Free Catalyst Award, and Life Science Investment Fund (LSIF, Maryland Technology Development Corporation). We thank Christopher D. Kontos for helpful comments.

Address correspondence to: Aleksander S. Popel, Department of Biomedical Engineering, Johns Hopkins University School of Medicine, 611 Traylor Research Building, 720 Rutland Avenue, Baltimore, Maryland 21205,USA. Phone: 410.955.6419; Email: apopel@jhu.edu. Or to: Niranjan B. Pandey, AsclepiX Therapeutics, Inc., 301 West 29th Street, Suite 2004, Baltimore, Maryland 21211, USA. Phone: 908.328.2019; Email: npandey4@jhmi.edu or npandey@asclepix.com.

1. Campochiaro PA. Molecular pathogenesis of retinal and choroidal vascular diseases. *Prog Retin Eye Res*. 2015;49:67–81.
2. Azzi S, Hebda JK, Gavard J. Vascular permeability and drug delivery in cancers. *Front Oncol*. 2013;3:211.
3. Zgraggen S, Ochsenbein AM, Detmar M. An important role of blood and lymphatic vessels in inflammation and allergy. *J Allergy (Cairo)*. 2013;2013:672381.

4. Durrani OM, Meads CA, Murray PI. Uveitis: a potentially blinding disease. *Ophthalmologica*. 2004;218(4):223–236.
5. Eklund L, Kangas J, Saharinen P. Angiopoietin-Tie signalling in the cardiovascular and lymphatic systems. *Clin Sci*. 2017;131(1):87–103.
6. Saharinen P, Eklund L, Alitalo K. Therapeutic targeting of the angiopoietin-TIE pathway. *Nat Rev Drug Discov*. 2017;16(9):635–661.
7. Davis S, et al. Isolation of angiopoietin-1, a ligand for the TIE2 receptor, by secretion-trap expression cloning. *Cell*. 1996;87(7):1161–1169.
8. Saharinen P, et al. Angiopoietins assemble distinct Tie2 signalling complexes in endothelial cell-cell and cell-matrix contacts. *Nat Cell Biol*. 2008;10(5):527–537.
9. Frye M, et al. Interfering with VE-PTP stabilizes endothelial junctions in vivo via Tie-2 in the absence of VE-cadherin. *J Exp Med*. 2015;212(13):2267–2287.
10. Dalton AC, Shlamkovitch T, Papo N, Barton WA. Constitutive Association of Tie1 and Tie2 with Endothelial Integrins is Functionally Modulated by Angiopoietin-1 and Fibronectin. *PLoS ONE*. 2016;11(10):e0163732.
11. Fiedler U, et al. The Tie-2 ligand angiopoietin-2 is stored in and rapidly released upon stimulation from endothelial cell Weibel-Palade bodies. *Blood*. 2004;103(11):4150–4156.
12. Maisonpierre PC, et al. Angiopoietin-2, a natural antagonist for Tie2 that disrupts in vivo angiogenesis. *Science*. 1997;277(5322):55–60.
13. Benest AV, et al. Angiopoietin-2 is critical for cytokine-induced vascular leakage. *PLoS ONE*. 2013;8(8):e70459.
14. Tabruyn SP, et al. Angiopoietin-2-driven vascular remodeling in airway inflammation. *Am J Pathol*. 2010;177(6):3233–3243.
15. Watanabe D, et al. Vitreous levels of angiopoietin 2 and vascular endothelial growth factor in patients with proliferative diabetic retinopathy. *Am J Ophthalmol*. 2005;139(3):476–481.
16. Korhonen EA, et al. Tie1 controls angiopoietin function in vascular remodeling and inflammation. *J Clin Invest*. 2016;126(9):3495–3510.
17. Cascone I, Napione L, Maniero F, Serini G, Bussolino F. Stable interaction between alpha5beta1 integrin and Tie2 tyrosine kinase receptor regulates endothelial cell response to Ang-1. *J Cell Biol*. 2005;170(6):993–1004.
18. Lee E, Lee SJ, Koskimaki JE, Han Z, Pandey NB, Popel AS. Inhibition of breast cancer growth and metastasis by a biomimetic peptide. *Sci Rep*. 2014;4:7139.
19. Silva RLE, et al. Tyrosine kinase blocking collagen IV-derived peptide suppresses ocular neovascularization and vascular leakage. *Sci Transl Med*. 2017;9(373):eaai8030.
20. Fukuhara S, et al. Differential function of Tie2 at cell-cell contacts and cell-substratum contacts regulated by angiopoietin-1. *Nat Cell Biol*. 2008;10(5):513–526.
21. Kim M, et al. Opposing actions of angiopoietin-2 on Tie2 signaling and FOXO1 activation. *J Clin Invest*. 2016;126(9):3511–3525.
22. Shen J, et al. Targeting VE-PTP activates TIE2 and stabilizes the ocular vasculature. *J Clin Invest*. 2014;124(10):4564–4576.
23. Hackett SF, Wiegand S, Yancopoulos G, Campochiaro PA. Angiopoietin-2 plays an important role in retinal angiogenesis. *J Cell Physiol*. 2002;192(2):182–187.
24. Oshima Y, et al. Different effects of angiopoietin-2 in different vascular beds: new vessels are most sensitive. *FASEB J*. 2005;19(8):963–965.
25. Han S, et al. Amelioration of sepsis by TIE2 activation-induced vascular protection. *Sci Transl Med*. 2016;8(335):335ra55.
26. Higgins SJ, et al. Tie2 protects the vasculature against thrombus formation in systemic inflammation. *J Clin Invest*. 2018;128(4):1471–1484.
27. Orfanos SE, et al. Angiopoietin-2 is increased in severe sepsis: correlation with inflammatory mediators. *Crit Care Med*. 2007;35(1):199–206.
28. Ziegler T, et al. Angiopoietin 2 mediates microvascular hemodynamic alterations in sepsis. *J Clin Invest*. 2013;123(8):3436–3445.
29. Chu CJ, et al. Multimodal analysis of ocular inflammation using the endotoxin-induced uveitis mouse model. *Dis Model Mech*. 2016;9(4):473–481.
30. Veevers-Lowe J, Ball SG, Shuttleworth A, Kielty CM. Mesenchymal stem cell migration is regulated by fibronectin through α5β1-integrin-mediated activation of PDGFR-β and potentiation of growth factor signals. *J Cell Sci*. 2011;124(Pt 8):1288–1300.
31. Rahman S, et al. Novel hepatocyte growth factor (HGF) binding domains on fibronectin and vitronectin coordinate a distinct and amplified Met-integrin induced signalling pathway in endothelial cells. *BMC Cell Biol*. 2005;6(1):8.
32. Chen TT, Luque A, Lee S, Anderson SM, Segura T, Iruela-Arispe ML. Anchorage of VEGF to the extracellular matrix conveys differential signaling responses to endothelial cells. *J Cell Biol*. 2010;188(4):595–609.
33. Soldi R, Mitola S, Strasly M, Defilippi P, Tarone G, Bussolino F. Role of alphavbeta3 integrin in the activation of vascular endothelial growth factor receptor-2. *EMBO J*. 1999;18(4):882–892.
34. Caswell PT, Chan M, Lindsay AJ, McCaffrey MW, Boettiger D, Norman JC. Rab-coupling protein coordinates recycling of alpha5beta1 integrin and EGFR1 to promote cell migration in 3D microenvironments. *J Cell Biol*. 2008;183(1):143–155.
35. Reynolds AR, et al. Stimulation of tumor growth and angiogenesis by low concentrations of RGD-mimetic integrin inhibitors. *Nat Med*. 2009;15(4):392–400.
36. Baron V, Schwartz M. Cell adhesion regulates ubiquitin-mediated degradation of the platelet-derived growth factor receptor beta. *J Biol Chem*. 2000;275(50):39318–39323.
37. Yu X, et al. Structural basis for angiopoietin-1-mediated signaling initiation. *Proc Natl Acad Sci USA*. 2013;110(18):7205–7210.
38. Kim KT, et al. Oligomerization and multimerization are critical for angiopoietin-1 to bind and phosphorylate Tie2. *J Biol Chem*. 2005;280(20):20126–20131.
39. Hakanpaa L, et al. Endothelial destabilization by angiopoietin-2 via integrin β1 activation. *Nat Commun*. 2015;6:5962.
40. Jahangiri A, et al. Cross-activating c-Met/β1 integrin complex drives metastasis and invasive resistance in cancer. *Proc Natl Acad Sci USA*. 2017;114(41):E8685–E8694.
41. Isaji T, Sato Y, Fukuda T, Gu J. N-glycosylation of the I-like domain of beta1 integrin is essential for beta1 integrin expression and biological function: identification of the minimal N-glycosylation requirement for alpha5beta1. *J Biol Chem*. 2009;284(18):12207–12216.
42. Isaji T, et al. N-glycosylation of the beta-propeller domain of the integrin alpha5 subunit is essential for alpha5beta1 heterodi-

merization, expression on the cell surface, and its biological function. *J Biol Chem*. 2006;281(44):33258–33267.
43. Felcht M, et al. Angiopoietin-2 differentially regulates angiogenesis through TIE2 and integrin signaling. *J Clin Invest*. 2012;122(6):1991–2005.
44. Askari JA, Buckley PA, Mould AP, Humphries MJ. Linking integrin conformation to function. *J Cell Sci*. 2009;122(Pt 2):165–170.
45. Mahabeleshwar GH, Chen J, Feng W, Somanath PR, Razorenova OV, Byzova TV. Integrin affinity modulation in angiogenesis. *Cell Cycle*. 2008;7(3):335–347.
46. Saharinen P, Eklund L, Alitalo K. Therapeutic targeting of the angiopoietin-TIE pathway. *Nat Rev Drug Discov*. 2017;16(9):635–661.
47. La Porta S, et al. Endothelial Tie1-mediated angiogenesis and vascular abnormalization promote tumor progression and metastasis. *J Clin Invest*. 2018;128(2):834–845.
48. Park JS, et al. Normalization of tumor vessels by Tie2 activation and Ang2 inhibition enhances drug delivery and produces a favorable tumor microenvironment. *Cancer Cell*. 2016;30(6):953–967.
49. Lampugnani MG, et al. The molecular organization of endothelial cell to cell junctions: differential association of plakoglobin, beta-catenin, and alpha-catenin with vascular endothelial cadherin (VE-cadherin). *J Cell Biol*. 1995;129(1):203–217.
50. Yuan JS, Wang D, Stewart CN. Statistical methods for efficiency adjusted real-time PCR quantification. *Biotechnol J*. 2008;3(1):112–123.
51. Bosch-Marce M, et al. Effects of aging and hypoxia-inducible factor-1 activity on angiogenic cell mobilization and recovery of perfusion after limb ischemia. *Circ Res*. 2007;101(12):1310–1318.
52. Shih SC, Ju M, Liu N, Smith LE. Selective stimulation of VEGFR-1 prevents oxygen-induced retinal vascular degeneration in retinopathy of prematurity. *J Clin Invest*. 2003;112(1):50–57.
53. Xu G, Zhang Y, Zhang L, Ren G, Shi Y. The role of IL-6 in inhibition of lymphocyte apoptosis by mesenchymal stem cells. *Biochem Biophys Res Commun*. 2007;361(3):745–750.